

Composition and lipid spatial distribution of HDL particles in subjects with low and high HDL-cholesterol[§]

Laxman Yetukuri,* Sanni Söderlund,[†] Artturi Koivuniemi,[§] Tuulikki Seppänen-Laakso,* Perttu S. Niemelä,* Marja Hyvönen,** Marja-Riitta Taskinen,[†] Ilpo Vattulainen,^{§,††,§§} Matti Jauhiainen,^{***,†††} and Matej Orešič^{1,*,*†††}

VTT Technical Research Centre of Finland,* Espoo, Finland, Division of Cardiology,[†] Department of Medicine, University of Helsinki, Helsinki, Finland, Department of Physics,[§] Tampere University of Technology, Tampere, Finland, Department of Physics,** University of Oulu, Finland, Department of Physics,^{††} Aalto University School of Science and Engineering, Espoo, Finland, MEMPHYS – Center for Biomembrane Physics,^{§§} University of Southern Denmark, Odense, Denmark, National Institute for Health and Welfare,^{***} Helsinki, Finland, Institute for Molecular Medicine Finland (FIMM),^{†††} Helsinki, Finland

Abstract A low level of high density lipoprotein cholesterol (HDL-C) is a powerful risk factor for cardiovascular disease. However, despite the reported key role of apolipoproteins, specifically, apoA-I, in HDL metabolism, lipid molecular composition of HDL particles in subjects with high and low HDL-C levels is currently unknown. Here lipidomics was used to study HDL derived from well-characterized high and low HDL-C subjects. Low HDL-C subjects had elevated triacylglycerols and diminished lysophosphatidylcholines and sphingomyelins. Using information about the lipid composition of HDL particles in these two groups, we reconstituted HDL particles *in silico* by performing large-scale molecular dynamics simulations. In addition to confirming the measured change in particle size, we found that the changes in lipid composition also induced specific spatial distributions of lipids within the HDL particles, including a higher amount of triacylglycerols at the surface of HDL particles in low HDL-C subjects. **¶** Our findings have important implications for understanding HDL metabolism and function. For the first time we demonstrate the power of combining molecular profiling of lipoproteins with dynamic modeling of lipoprotein structure.—Yetukuri, L., S. Söderlund, A. Koivuniemi, T. Seppänen-Laakso, P. S. Niemelä, M. Hyvönen, M-R. Taskinen, I. Vattulainen, M. Jauhiainen, and M. Orešič. **Composition and lipid spatial distribution of HDL particles in subjects with low and high HDL-cholesterol.** *J. Lipid Res.* 2010. 51: 2341–2351.

Supplementary key words high density lipoprotein • lipidomics • lipid metabolism • molecular dynamics

This work was supported by the European Union-funded project ETHERPATHS (FP7-KBBE-222639) (<http://www.etherpaths.org/>), the Finnish Heart Foundation, the Sigrid Juselius Foundation, and the Helsinki University Central Hospital Research Foundation.

Manuscript received 2 March 2010 and in revised form 27 April 2010.

Published, JLR Papers in Press, April 27, 2010
DOI 10.1194/jlr.M006494

Copyright © 2010 by the American Society for Biochemistry and Molecular Biology, Inc.

This article is available online at <http://www.jlr.org>

High-density lipoprotein (HDL) is one of the five major lipoproteins (chylomicrons, VLDL, IDL, LDL, and HDL). HDL is the smallest and densest of the lipoproteins because it contains the highest proportion of protein. A low level of HDL cholesterol (HDL-C) is a powerful risk factor for cardiovascular disease (1–3). Accumulating evidence suggests, however, that HDL-C alone may not be an adequate marker of atheroprotection. HDLs are compositionally and functionally diverse lipoprotein particles, and this diversity needs to be taken into account in the evaluation of cardiovascular risk (4, 5). A recent study of HDL proteome revealed many important changes in the protein composition of HDL in cardiovascular patients without changes in serum HDL-C (6).

Detailed characterization of lipoprotein fractions and changes in their molecular lipid profiles may help identify novel biomarkers in lipid metabolism (7). Main lipid constituents of HDL particles include glycerophospholipids, cholesteryl esters (ChoE), sphingomyelins (SM), and triacylglycerols (TG). Lysophosphatidylcholines (lysoPC) are known to be associated with proatherogenic conditions (8). Enrichment of HDL phospholipids, such as phosphatidylcholines (PC) and SM, improves the net efflux of

Abbreviations: Apo, apolipoprotein; CETP, cholesteryl ester transfer protein; ChoE, cholesteryl ester; CRP, C-reactive protein; FCho, free cholesterol; FDR, false discovery rate; HDL-C, high-density lipoprotein cholesterol; IL, interleukin; LDL-C, low-density lipoprotein cholesterol; lysoPC, lysophosphatidylcholine; MS, mass spectrometry; PC, phosphatidylcholine; PE, phosphatidylethanolamine; PLS/DA, partial least square discriminant analysis; PLTP, phospholipid transfer protein; RCT, reverse cholesterol transport; SM, sphingomyelin; TG, triacylglycerol; TNF, tumor necrosis factor; UPLC, ultra performance liquid chromatography.

¹To whom correspondence should be addressed.

e-mail: matej.oresic@vtt.fi

§ The online version of this article (available at <http://www.jlr.org>) contains supplementary data in the form of three tables and ten figures.

cholesterol from scavenger receptor-BI expressing cells (9), and phospholipid composition may have a major impact in the process of reverse cholesterol transport (RCT) (10). We also demonstrated using HDL derived either from low or high HDL-C subjects that cholesterol efflux from human THP-1 macrophages correlated with phospholipids, particle size, and particle mass of HDL (11). This is consistent with earlier efflux studies demonstrating that the phospholipid content of HDL is an important determinant of cholesterol egress (12, 13). Additionally, the activity of HDL in the first step of RCT is affected by the fatty acyl chain length of the phospholipids (14). Together, the information on lipid molecular composition of HDL may provide better insights into the mechanisms behind the anti-atherogenic role of HDL particles.

Conventional lipoprotein analyses have relied on analyses of total protein, phospholipid, free cholesterol, ChoE, and TG content (15). However, molecular level concentrations may provide more precise markers of specific metabolic phenotypes than total lipid class concentrations (16). Recent advances in mass spectrometry (MS)-based analytical platforms and bioinformatic approaches for managing large volumes of data have made it possible to study lipid species at the molecular level (17, 18). The lipidomics platform based on ultra performance liquid chromatography mass spectrometry (UPLC/MS) was recently utilized to characterize molecular lipids, including triacylglycerols, glycerophospholipids, sphingomyelins, cholesteryl esters, and ceramides in different lipoprotein fractions (16).

Lipid molecular composition of HDL particles in subjects with high and low HDL-cholesterol levels has not been studied systematically. Here we combine clinical cohort study and global lipidomics with molecular simulations of HDL particles. We apply UPLC/MS-based lipidomics to study HDL fractions from well-characterized high and low HDL-C subjects from a large Finnish population cohort, and we identify many specific changes in HDL lipidomes among subjects with high and low HDL-C. Using information about the lipid composition of HDL particles in these two groups, we reconstitute HDL particles *in silico* by performing large-scale molecular dynamics simulations. In addition to confirming the measured change in particle size, we show that HDL particles derived from high HDL-C subjects have a surprisingly different spatial distribution of triacylglycerols.

MATERIALS AND METHODS

Study subjects

The study comprised 47 subjects: 24 low HDL subjects and 23 high HDL subjects who were participants in the Health 2000 Health Examination Survey (19). The subjects represented the extreme ends of HDL-C levels (≤ 10 th percentile and ≥ 90 th percentile). HDL-C limits were as follows: low HDL-C men ≤ 1.03 mmol/l, low HDL-C women ≤ 1.23 mmol/l, high HDL-C men ≥ 1.79 mmol/l, and high HDL-C women ≥ 2.24 mmol/l. Subjects with diabetes, alcohol abuse, or malignancy were excluded. Alcohol abuse was defined as >160 g of alcohol per week for women and >310 g of alcohol per week for men. In addition, subjects

using systemic estrogen, corticosteroid therapy, statins, or other drugs affecting HDL metabolism were excluded. Each study subject gave a written informed consent before participating in the study. The samples were collected in accordance with the Helsinki declaration, and the ethics committees of the participating centers approved the study design. **Table 1** presents the characteristics of the low and high HDL-C subjects.

Lipoprotein separation and characterization

HDL for the lipidomic analysis was separated from plasma samples by ultracentrifugation (20). HDL subspecies distribution and HDL mean particle size were determined with native gradient gel electrophoresis (21) with minor modifications as previously described (11). The molecular size intervals for HDL subspecies 2b, 2a, 3a, 3b, and 3c were used according to Blanche et al. (21), and for each subspecies, the relative area under the densitometric scan were reported. HDL mean particle size was calculated by multiplying the mean size of each HDL subclass by its relative area under the densitometric scan (22). LDL peak particle size was measured with gradient gel electrophoresis as previously described in detail (23).

Biochemical analyses

Venous blood samples were drawn after an overnight fast. Serum and EDTA plasma samples were stored at -70°C before analysis. Serum total cholesterol (TC), TG, and HDL-C were measured with Olympus AU400 clinical chemistry analyzer (Olympus, Hamburg, Germany) by fully enzymatic methods (Olympus kits OSR 6116 and 6133 for TC and TG, respectively, and Roche Diagnostics kit 3030024 for HDL-C) (Roche Diagnostics GmbH, Mannheim, Germany). LDL-C was calculated using the Friedewald formula (24). Concentrations of apoA-I and apolipoprotein B (apoB) were measured with Olympus AU400 analyzer by immunoturbidometric methods (kits 64265 and 67249 from Orion Diagnostica, Espoo, Finland). Serum apolipoprotein A-II (apoA-II) was measured with Cobas Mira analyzer (Hoffman-La Roche, Basel, Switzerland) immunoturbidometrically (Wako Chemicals GmbH, Neuss, Germany, and own polyclonal antibody produced in rabbits against purified human apoA-II). Serum apoE concentration was quantitated by ELISA (25). Plasma glucose was measured by the glucose dehydrogenase method (Merck Diagnostica, Darmstadt, Germany). Plasma insulin was measured by radioimmunoassay (Pharmacia AB, Uppsala, Sweden).

Phospholipid transfer protein (PLTP) activity was measured using the radiometric assay as previously described (26) with minor modifications (27). PLTP concentration was measured with ELISA (28). Cholesterol ester transfer protein (CETP) activity was measured with radiometric assay as described by Groener et al. (29). Paraonase activity was measured with spectrophotometry (30). Nitrotyrosine concentration was measured with ELISA using kit HK 501 (HyCult Biotechnology, Uden, The Netherlands). The measurements of interleukin-6 (IL-6), tumor necrosis factor- α (TNF- α), and C-reactive protein (CRP) were done using the immuno-chemiluminometric assay (Immulite, DPC, Siemens Healthcare Diagnostics, USA).

Blood pressure values are the mean values from three consecutive measurements carried out in 1–2 min intervals. Data on alcohol consumption was collected from questionnaires filled in by the study subjects.

Lipidomic analysis

An internal standard mixture containing 10 lipid compounds was added to each sample (20 μl of total HDL fraction). Lipids were extracted with chloroform/methanol (2:1, v/v, 100 μl) solvent. The samples were centrifuged (10000 rpm, 3 min), 60 μl of the lower lipid extract was taken into an HPLC vial insert, and

TABLE 1. Clinical and biochemical characteristics of the study subjects

	Low HDL Subjects (Median IQR)	High HDL Subjects (Median IQR)	<i>P</i> ^a
N (men/women) ^b	24 (12/12)	23 (12/11)	
Age (years)	53 (51–56)	54 (50–60)	0.564
Body mass index (kg/m ²)	27.9 (24.3–31.5)	22.8 (21.4–24.6)	<0.001
Systolic blood pressure (mmHg)	131 (118–146)	132 (121–147)	0.647
Diastolic blood pressure (mmHg)	81 (75–89)	81 (75–87)	0.882
Total cholesterol (mmol/l)	5.15 (4.55–5.60)	5.80 (5.30–6.10)	<0.001
HDL cholesterol (mmol/l)	0.94 (0.86–1.10)	2.52 (2.12–2.61)	<0.001
LDL cholesterol (mmol/l)	3.30 (2.87–3.67)	3.01 (2.68–3.55)	0.225
Insulin (mU/l)	9.15 (7.05–10.93)	6.00 (5.00–7.90)	0.0015
Triglycerides (mmol/l)	1.80 (1.23–2.25)	0.70 (0.60–0.90)	<0.001
apoA-I (mg/dl)	134 (121–144)	222 (206–234)	<0.001
apoA-II (mg/dl)	28.0 (27.0–34.5)	39.0 (35.0–45.0)	<0.001
apoB (mg/dl)	124.5 (106.3–135.0)	99.0 (84.0–109.0)	<0.001
PLTP activity (nmol/ml/h)	4765 (4109–5549)	5304 (4798–5810)	0.058
PLTP mass (µg/ml)	7.5 (6.4–9.2)	8.6 (6.8–9.5)	0.328
CETP activity (nmol/ml/h)	28 (25–33)	31 (27–38)	0.250
TNF-α (ng/l)	6.5 (4.5–8.2)	4.7 (4.1–5.8)	0.038
IL-6 (ng/l)	1.6 (1.0–2.1)	1.1 (0.8–2.0)	0.163
hs-CRP (mg/l)	1.4 (0.8–2.7)	0.7 (0.4–1.2)	0.012
HDL size (nm)	9.0 (8.8–9.2)	9.9 (9.7–10.2)	<0.001

Abbreviations: Apo, apolipoprotein; CETP, cholesteryl ester transfer protein; hs-CRP, high sensitivity C-reactive protein; IL, interleukin; IQR, interquartile range; PLTP, phospholipid transfer protein; TNF, tumor necrosis factor.

^a *P*-value from Mann-Whitney *U* test.

^b apoA-II measurements of three subjects in both low and high HDL-C groups are not available; hence, calculations are based on measurements from the remaining subjects.

another standard mixture containing three labeled lipid compounds was added. The internal standards include PC(17:0/0:0), PC (17:0/17:0), PE(17:0/17:0), PG(17:0/17:0) [rac], Cer(d18:1/17:0), PS(17:0/17:0), PA(17:0/17:0) and D-erythro-Sphingosine-1-Phosphate (C17 Base) from Avanti Polar Lipids (Alabaster, AL) and MG(17:0/0:0/0:0) [rac], DG(17:0/17:0/0:0) [rac], and TG(17:0/17:0/17:0) from Larodan Fine Chemicals (Malmö, Sweden). The labeled standards include PC(16:0/0:0-D3), PC(16:0/16:0-D6), and TG(16:0/16:0/16:0-¹³C3) from Larodan Fine Chemicals.

Lipid extracts (2 µl injections) were analyzed on a Waters Q-ToF Premier mass spectrometer combined with an Acquity Ultra Performance LC™ (UPLC™) (Waters Inc., Milford, MA). The column was an Acquity UPLC BEH C18 10 × 50 mm with 1.7 µm particles and the gradient solvent system included water (1% 1M NH₄Ac, 0.1% HCOOH) and LC/MS grade (Rathburn) acetonitrile/isopropanol (5:2, 1% 1M NH₄Ac, 0.1% HCOOH). The total run time, including a 5 min reequilibration step, was 18 min. The flow rate was 0.200 ml/min. The data were collected at mass range of *m/z* 300–1200 with a scan duration of 0.2 s in ESI+ mode.

Statistical methods

Statistical analyses were performed using a freely available R language (<http://www.r-project.org/>). False discovery rate (FDR) *q*-values were computed using statistical methods from R package “*qvalue*.” Correlation analysis was performed using “*gplots*” library from R package.

Chemometric modeling of data

Supervised model was built for clustering and discrimination using partial least squares discriminant analysis (PLS/DA) (31, 32). The PLS/DA model attempts to get the latent variables by maximizing the covariance between measured data (X) (e.g., lipid profile data) and response variables of interest (Y) (e.g., high HDL-C and low HDL-C groups). The model was built by scaling X data to unit variance and zero mean, and Y data to zero mean. The random subsets cross validation method (33) and Q²

scores were used to optimize the models. The variable importance in the projection (VIP) values (34) were computed to identify most important lipid species contributing to separation of low and high HDL-C groups in the PLS/DA model. PLS/DA model was built using Matlab, version 7.0 (Mathworks, Natick, MA) and PLS Toolbox, version 4.0, of the Matlab package (Eigenvector Research, Wenatchee, WA).

Construction of simulation systems and simulation parameters

In the case of apoA-I, we first built an all-atom model for apoA-I based on the previous data, and then we coarse grained the structure. The relative conformation of apoA-I was similar to the belt-like structure of Borhani et al. who produced the solution X-ray structure of truncated apoA-I (residues 44–243) (35). We also followed the approach of Segrest et al. who arranged atomistic apoA-I around the lipid moiety in belt-like fashion (36) so that the hydrophobic sides of amphiphilic α-helices were pointing toward the lipid moiety. This structure was further used to build a model for the full-length apoA-I by adding the previously absent N-terminal part (residues 1–43) of the apoA-I to our model. The conformation of this segment was determined to be α-helical as suggested by the previous NMR data (37). The hydrophobic side of this helix was also orientated toward the lipid moiety. We directly coarse grained the atomistic structure and placed the apoA-I around the previously simulated lipid droplet. The secondary structure of apoA-I was enforced almost completely to the α-helical conformation; only the N- and C-terminal ends were modeled as random coils. This approach has been used previously in the work of Catte et al. with truncated apoA-I (38). Thus, the flexibility of α-helical segments arises from the three-body angle and four-body dihedral potentials of backbone beads that were produced by Monticelli et al. to extend the MARTINI force field to proteins (39). The radius of the ring formed by apoA-I was ~12.5 nm, and the average distance between apoA-I was 2.5–3.0 nm.

Next, to produce starting structures for the low HDL-C, normal HDL-C, and high HDL-C systems, the lipid composition of

the previously simulated lipid droplet was tuned according to **Table 2**. All lipid molecules, except those that were added to the starting system, were inside the ring formed by apoA-I. Next all three systems were energy minimized by the steepest descent algorithm, and 10 ns vacuum simulations were carried out to get lipids to the one unified phase, which meant that the added lipids diffused to the main lipid particle. Systems were solvated, and 18 water beads were changed to Na⁺ beads to neutralize the charges in the systems. Production simulations lasted for 2 μs, which corresponds to 8 μs of effective time as the MARTINI model speeds up the dynamics by an approximate factor of four (39). System sizes were approximately 30,000–35,000 water beads and 4,300–5,000 lipid and protein beads in total. The box size in each simulation was 17 × 17 × 17 nm.

Simulations were performed by the GROMACS simulation package (v. 4.0) (40). The standard MARTINI lipid force field was used for PC (PC(16:0/18:1)), lysoPC (PC(16:0/0:0)), FCho, and SM (SM(d18:1/16:0)) molecules (41). Protein part was modeled using the protein extension of the MARTINI description (39). TG (TG(18:1/18:1/18:1)) and ChoE (ChoE(18:1)) force fields were constructed based on the philosophy of MARTINI force field (the exact parameters and validation are available elsewhere (38)). In all simulations, temperature was set to 310 K and pressure to 1 bar. Berendsen temperature and pressure coupling algorithms (42) were utilized with coupling constants of 0.4 ps and 2.0 ps, respectively. All lipid classes, apoA-I, water, and ions were separately coupled to heat bath. Electrostatic and Lennard-Jones interactions were calculated using the shift type potentials with cut-off lengths of 1.2 nm, and the potentials were shifted to zero starting at 0.0 and 0.9 nm, respectively. Time step was set to 0.025 ps. In each case, the first 4 μs were treated as equilibration simulation; the last 4 μs were used in the analysis. GROMACS analysis programs g_rdf, g_mindist, g_gyrate, and g_rmsf were used in the analysis.

RESULTS

Characteristics of the study subjects

Clinical and biochemical characteristics of low and high HDL-C subjects are shown in Table 1. As expected, the high HDL-C subjects had higher fasting serum HDL-C ($P < 0.001$) and total cholesterol ($P < 0.001$) concentrations compared with low HDL-C subjects. However, fasting serum LDL-C concentrations between the groups did not differ significantly. High HDL-C subjects were leaner compared with low HDL-C subjects, and they had lower body

mass index ($P < 0.001$), lower triglyceride ($P < 0.001$) and insulin ($P = 0.0015$), as well as lower TNF-α ($P = 0.038$) and hs-CRP ($P = 0.012$) levels in plasma. The two groups had similar PLTP mass and CETP activity levels (Table 1). As expected, high HDL-C subjects had higher apoA-I ($P < 0.001$) and lower apoB ($P < 0.001$) values than low HDL-C subjects.

Lipidomic profiling of HDL fractions

To characterize the HDL-associated lipids at the molecular level, the established lipidomics platform using UPLC/MS was applied as described previously (43). A total of 307 molecular lipids across 12 functional classes were detected. PLS/DA revealed that the HDL lipidomic profiles in low HDL-C and high HDL-C subjects are clearly different (**Fig. 1A**). As shown by clustering of the top-ranked discriminant lipids in Fig. 1B, the HDL compositional changes in high HDL-C subjects compared with low HDL-C subjects were dominated by elevated lysoPCs, SMs, and ChoEs, and diminished TGs. No within-class trend was observed between the low and high HDL-C groups for PCs. Box plots for the most abundant lipids from lysoPC, SM, ChoE, ethanolamine plasmalogen (PEp) and TG classes are shown in **Fig. 2**. The most significant identified lipid species with their fold changes and FDR q -values are shown in supplemental Table I. Full lipidomics results for 307 detected lipid peaks are shown in supplemental Table II. The observed, highly significant differences between the HDL lipidomic profiles of the high and low HDL-C groups were not attributed to gender (supplemental Fig. I) or TG fatty acid composition (supplemental Fig. II), despite the observed gender differences in HDL subspecies distribution in the low HDL-C group (supplemental Table III).

Although not among the most abundant HDL phospholipids, several of the ether lipids were found among the most significantly different in high and low HDL groups (Fig. 1 and supplemental Table II), including the ethanolamine plasmalogens PE(P-16:0/18:2), PE(P-16:0/20:4), and PE(P-18:1/20:4) (supplemental Table II). The ethanolamine plasmalogens as well as PC ether lipids containing high number of double bonds were diminished in the high HDL group, while the more saturated ether PCs were

TABLE 2. Lipid compositions and concentrations used in simulations

	Lipid Compositions ^a Determined by Lipidomics						
	apoA-I	SM	PC	FCho	ChoE	TG	lysoPC
Normal HDL-C	2	18	109	50	90	19	10
Low HDL-C	2	13	109	25	81	24	5
High HDL-C	2	23	109	75	99	14	15
	Average Concentrations ^b of Lipid Classes Determined by Lipidomics						
	SM	HDL-C	ChoE	TG	lysoPC		
Low HDL-C	0.057 ± 0.003	7.545 ± 0.200	0.105 ± 0.009	0.436 ± 0.024	0.014 ± 0.007		
High HDL-C	0.082 ± 0.004	10.928 ± 0.254	0.132 ± 0.020	0.244 ± 0.036	0.022 ± 0.002		

Abbreviations: Apo, apolipoprotein; ChoE, cholesteryl ester; FCho, free cholesterol; HDL-C, high-density lipoprotein cholesterol; LDL-C, low-density lipoprotein cholesterol; lysoPC, lysophosphatidylcholine; SM, sphingomyelin; TG, triacylglycerol.

^a Number of molecules per HDL particle.

^b Units are μmol/l [lipid] / mg/dl [apoA-I].

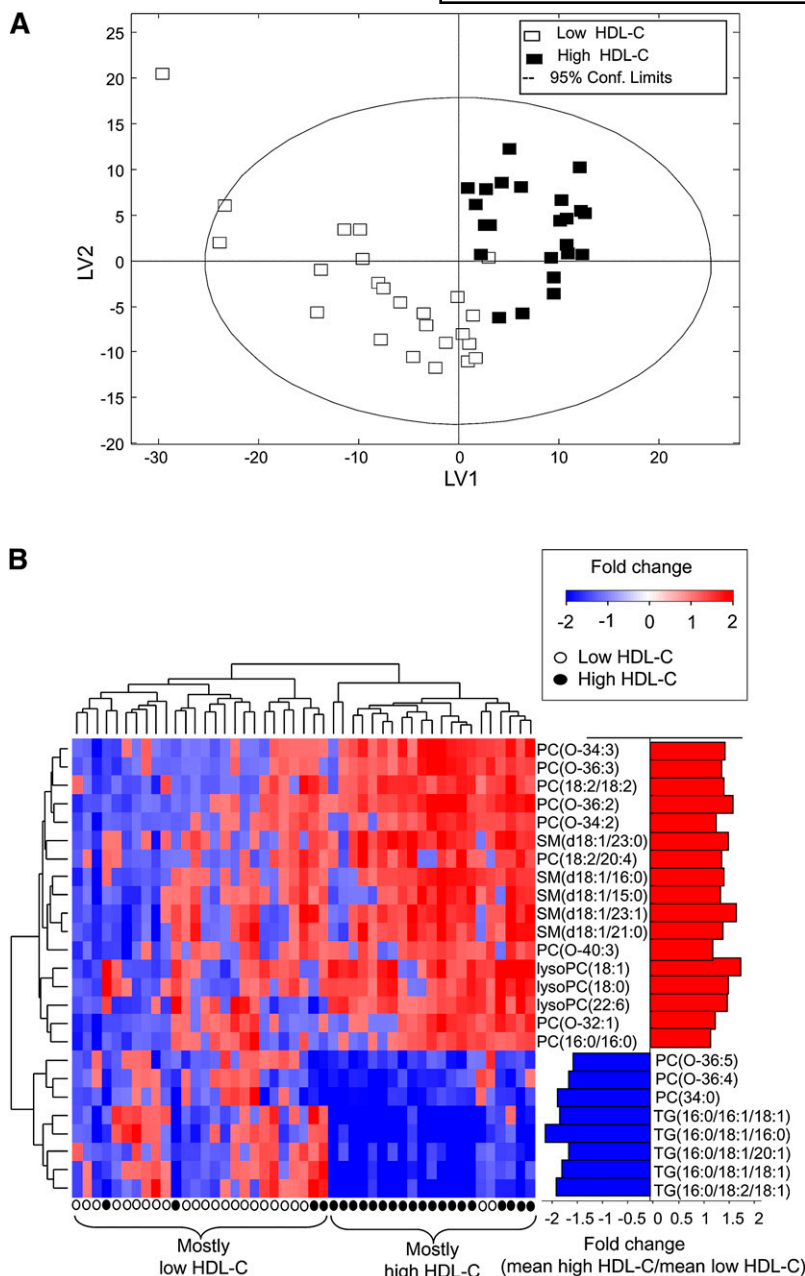


Fig. 1. A: Partial least squares discriminant analysis (PLS/DA) of lipidomic profiles for low HDL-C and high HDL-C subjects. PLS/DA scores plot with two latent variables were used ($Q^2 = 51\%$). B: Hierarchical clustering on most important variable importance in the projection (VIP) variables and samples in the heat map reflecting fold changes of lipids relative to mean intensity within the low HDL-C group. Bars show fold changes reflecting mean intensity of top VIP variables in the high HDL-C group relative to mean intensity within the low HDL-C group.

elevated compared with the levels in the low HDL group. The top-ranked lipids derived from PLS/DA (Fig. 1A) were correlated with the selected clinical variables (supplemental Fig. III). TG concentrations were negatively correlated while SM and lysoPC concentrations were positively correlated with the HDL-C concentration.

We then investigated association of HDL-C with the top-ranked lipids from different lipid classes in low and high HDL-C subjects separately (supplemental Figs. IV and V). Positive correlations between SM(d18:1/16:0) and HDL-C were similar in low HDL-C subjects ($r = 0.71$, $P = 0.0001$) and high HDL-C subjects ($r = 0.71$, $P = 0.0001$). Interestingly, positive correlation identified between lysoPC(18:0) and HDL-C in low HDL-C subjects ($r = 0.54$, $P = 0.006$) was absent in the high HDL-C group ($r = -0.06$, $P = 0.78$). We observed no correlation of TG(16:0/18:1/20:1) with HDL-C in low HDL-C subjects ($r = 0.06$, $P = 0.75$), whereas there

was a negative correlation in high HDL-C subjects ($r = -0.43$, $P = 0.04$). No significant correlations were found between ChoE(18:1) and HDL-C, in either low HDL-C subjects ($r = 0.33$, $P = 0.12$) or high HDL-C subjects ($r = 0.02$, $P = 0.92$). Correlation analysis was also performed for the HDL particle size versus the selected lipids (supplemental Figs. IV and V). HDL particle size correlated positively with lysoPC(18:0) ($r = 0.50$, $P = 0.0003$) and SM(d18:1/16:0) ($r = 0.58$, $P = 0.0003$), and negatively with TG(16:0/18:1/20:1) ($r = -0.51$, $P < 0.0001$). No such significant correlations were observed when analyzing the low and high HDL-C groups separately.

Simulations of HDL particles

Our findings imply that the lipid composition of HDL particles derived from subjects with high and low HDL cholesterol is very different. To gain further insight how the

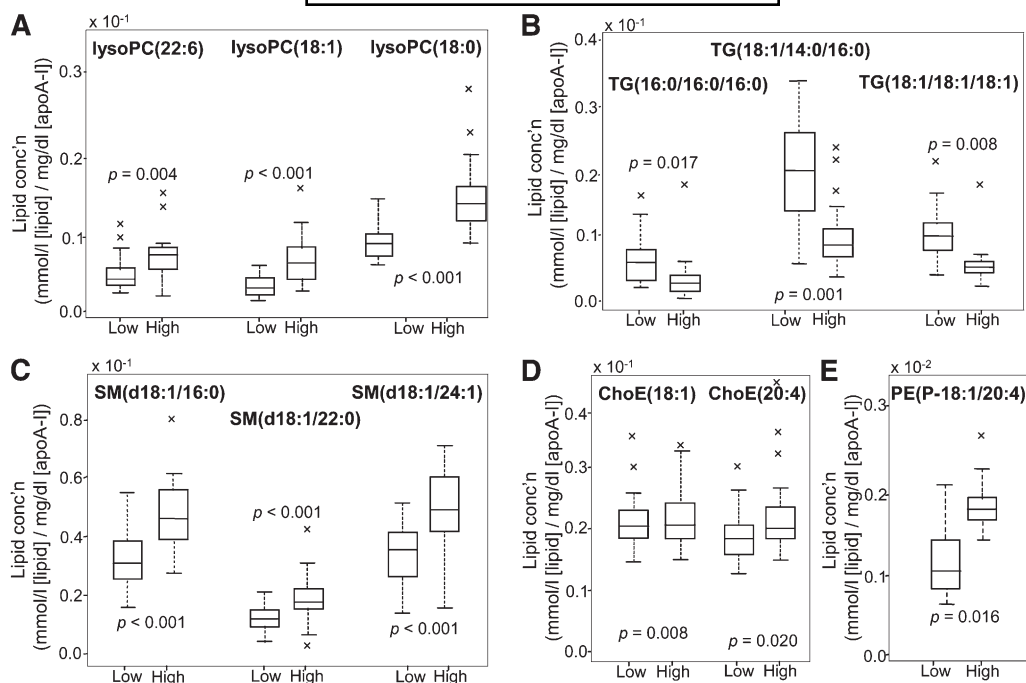


Fig. 2. Box plots of the most abundant lipids within the TG, lysoPC, SM, ChoE, and ethanolamine plasmalogen (PEp) classes. Concentrations are shown in $\mu\text{mol/l}$ [lipid] / mg/dl [apoA-I]. High, high HDL-C; Low, low HDL-C. ChoE, cholesteryl ester; lysoPC, lysophosphatidylcholine; SM, sphingomyelin; TG, triacylglycerol.

changes in the lipid composition of HDL may influence HDL structure and function, we performed coarse-grained simulations of HDL particles, with their molecular composition derived from within-group mean selected lipid concentrations obtained by lipidomics. Three coarse-grained molecular dynamic simulations with different lipid compositions were carried out. In addition to “high HDL-C” and “low HDL-C” particles, we simulated “normal HDL-C” as an intermediate between the two. The number of lipids used in each simulation is listed in Table 2. The lipid species concentrations obtained in global lipidomic profiling were expressed relative to the moles of apoA-I content. If lipid species in a certain class were contributing to separation of low and high HDL-C groups per the PLS/DA model, the averaged concentration of all species in that class was used to find the estimate of fold changes between low and high HDL-C groups. Alternatively, for the lipid species such as cholesteryl esters, which did not contribute much in the separation of the two HDL-C groups as per the model, the averaged concentration levels of all identified species were used to find the fold change estimate between the low and high HDL-C groups. Thus, obtained fold change values between low and high HDL-C groups were used to estimate the number of species per HDL particle in low and high HDL-C particles by comparing the numbers in the normal HDL-C compositions. The lipid composition for the normal-HDL model was chosen based on the previous article (44) that describes the detailed molecular composition of the HDL2-subfraction.

The size of simulated HDL particles decreased when moving from high to low HDL-C particles. This can be clearly seen from the radii of gyration (R_g) obtained from

the simulation (supplemental Fig. VI). To estimate the hydrodynamic particle radii (R_H), we used the relation ($R_g = \text{sqrt}(3/5) R_H$) for a uniform sphere. The hydrodynamic diameter of the high HDL-C particle was estimated to be 9.7 nm, and of the low HDL-C, 9.4 nm. As an indirect validation of our combined experimental and modeling strategy, the diameters calculated from simulations are in approximate agreement with our hydrodynamic particle diameters produced by electrophoresis, with the respective diameters of 9.9 and 9.0 nm when comparing high and low HDL-C particle profiles. One should note that the experimental size measurements include all HDL fractions, and thus, it is not directly comparable with our simulations. However, the results are within the right size range.

Interestingly, we registered by visual inspection that free cholesterol (Fcho) molecules accumulated next to apoA-I proteins, indicating that free cholesterol molecules interact more favorably with apoA-I (Fig. 3B). This interaction may have important implications for the HDL metabolism as the cholesterol molecule concentration in the particles can modulate the conformational fluctuations of apoA-I or even change it. Indeed, studies with human apoA-I have shown that cholesterol decreases the adsorption of the apolipoprotein to a phospholipid monolayer, and the conformation of apoA-I varies from one lipid monolayer to another, implying similar effects on the surface of HDL particles (45). It has been suggested that LCAT activity depends on the conformation of apoA-I (46, 47); thus, the cholesterol concentration could also be linked to the activation of LCAT and other HDL-associated proteins. Therefore, we calculated the number of contacts between

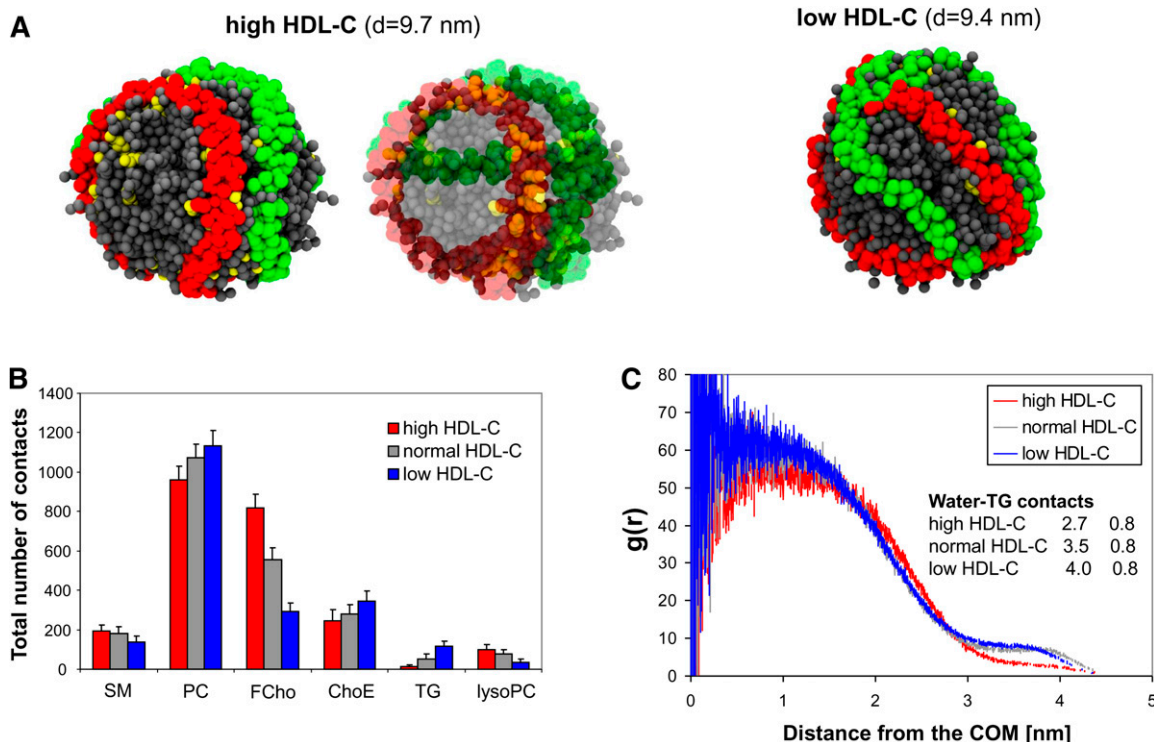


Fig. 3. Coarse-grained simulations of HDL particles reconstituted based on lipidomics data. **A:** Snapshots from the end of high and low HDL-C simulations (8 μ s). ApoA-I are colored with red and green, cholesterol molecules are yellow, and all other lipids are gray. Water phase was removed from the snapshots for clarity. Middle snapshot demonstrates how the cholesterol molecules are localized next to and under apoA-I in high HDL-C simulation. **B:** The number of contacts between apoA-I and different lipid beads in each simulation (error bars indicate \pm SD). The number of contacts was not normalized with the number of different lipid constituents. **C:** Radial distribution function for TG molecules $g(r)$ with respect to the center of mass (COM) of HDL particle. When surface lipid concentration decreases, more TGs are able to penetrate the surface monolayer, which is seen as a formation of higher plateaus near 3.5 nm. The number of contacts between TG and water beads (per TG) in different simulations is shown in the inset. Apo, apolipoprotein; TG, triacylglycerol.

different lipid species and apoA-I (Fig. 3B). Furthermore, we produced root mean square fluctuation (RMSF) curves for apoA-I in different cases to characterize differences in the local fluctuations (supplemental Fig. VII). The number of contacts increased between pairs SM-apoA-I, FCho-apoA-I, and lysoPC-apoA-I when moving from low HDL-C to high HDL-C (Fig. 3B). In contrast, the number of contacts decreased between pairs ChoE-apoA-I, TG-apoA-I, and PC-apoA-I. However, only the cholesterol molecules accumulate preferably next to apoA-I proteins independent of cholesterol concentration. This suggests that either the partitioning of cholesterol in HDL particles is entropy-driven or apoA-I possess high cholesterol affinity.

To study how the changes of lipid composition may affect the spatial distribution of specific lipid classes in HDL particles, we calculated the 3D radial distribution functions (RDF) for different lipid components with respect to the center of mass of HDL particles (Fig. 3C and supplemental Figs. VIII-X). Most notably, in low HDL-C the RDF of triacylglycerols indicated stronger prevalence of TG molecules at the surface (Fig. 3C) when the amount of cholesterol as well as other surface lipids decreases. The prevalence of cholesteryl esters did not change accordingly (supplemental Figs. VIII-X). Furthermore, we estimated the relative solubility TGs to the surface lipid monolayer by calculating the number of contacts between

TGs and water phase, divided by the number of TG molecules (Fig. 3C). The relative solubility of TG increased with fewer surface lipids in the HDL particles.

DISCUSSION

Our study revealed marked differences in HDL lipidomic profiles as well as related clinical and biochemical characteristics between low and high HDL-C subjects. For the first time, the molecular profiling of HDL (or other lipoprotein) particles was combined with dynamic structural modeling. Such an approach allowed us to show that the lipid compositional changes also induce specific spatial distributions of lipids within the HDL particles.

The composition of lipid and apolipoprotein components is critical in maintaining normal HDL metabolism as well as function. The HDL biosynthesis is very complex and associated with major steric and lipid interaction changes in structural apolipoproteins, such as apoA-I and apoA-II. ApoA-I, which constitutes about 70% of HDL protein content, is present in almost all HDL particles (48). The lack of the apoA-I gene is associated with low HDL-C levels in mice (49) and humans (50). This association is valid with our observations, with the low HDL-C subjects displaying lower levels of apoA-I as well as apoA-II, which constitutes approximately 20% of HDL protein (51).

The combined information from the key metabolic regulators and lipid profiles may provide the basis for mechanistic links in HDL metabolism. In addition to apoA-I and apoA-II, the key metabolic regulators, such as CETP, lecithin-cholesterol acyltransferase (LCAT), endothelial lipase (EL), hepatic lipase (HL), and PLTP, play a central role in continuous intravascular remodeling of HDL particles. ApoA-I acts as a cofactor for LCAT, the enzyme responsible for transforming the free cholesterol to cholesteryl ester in the core of HDL (52). As higher apoA-I levels closely associated with high HDL-C (48, 53), higher HDL-cholesteryl ester content was observed in high HDL-C subjects compared with low HDL-C groups (Fig. 2D). The cholesteryl esters in HDL are continuously exchanged for TG in very low-density lipoprotein (VLDL) or chylomicrons in a process mediated by CETP activity. Our findings revealed increases of TG content in HDL particles in low HDL-C subjects, thus favoring the active ChoE/TG exchange process. TG enrichment of HDL notably increases the ability of hepatic lipase to remodel these HDL particles (54, 55), resulting in release of lipid-poor apoA-I and enhanced clearance of HDL via the kidneys. It is known that cubilin acts as a receptor for the endocytosis of apoA-I in the kidney (56, 57).

Previous data suggest that in HDL particles the percentage of ChoEs of all surface lipids is 13–27% due to high tendency of ChoEs to locate on the surface and high concentration of ChoEs in these particles (58). Thus the known heteroexchange of ChoEs and TGs between HDL particles and apoB-100-containing lipoproteins is rational only if the acceptor and donor surfaces have different molar proportions of ChoE and TG (58). In addition, higher concentration of TG molecules at the surface of HDL particles could give a better chance for hepatic lipase to modify them.

The phospholipid content in HDL is regulated by PLTP, another important factor (59). Mice with mild overexpression of PLTP did not reveal significant changes in HDL, but those lacking PLTP have low HDL-C levels (60, 61). On the other hand, strong induction of PLTP expression strongly lowered total plasma HDL levels in a dose-dependent way because of accelerated fractional catabolism of HDL (62). In the present study, PLTP activities did not differ between the two HDL groups, suggesting that PLTP cannot be responsible for the low HDL levels. PLTP facilitates the transfer of phospholipids between lipoprotein particles and regulates both size and composition of HDL particles. The TG content of HDL has a major influence on PLTP-mediated size changes (63). The PLTP-mediated processes facilitate the transfer of surface remnants from lipolyzed triglyceride-rich lipoproteins to nascent HDL particles.

LCAT activation is influenced by the size of spherical HDL particles (64, 65). When the diameter of HDL particles increases the activity of LCAT enzyme is higher. Thus, we propose that the diameter of HDL particles is smaller in low HDL-C than in high HDL-C subjects. This lower activity could be somehow related to the conformation of apoA-I which could depend on the size and the lipid com-

position of the HDL particles. Interestingly, sphingomyelin content of HDL particles has been reported to affect LCAT activity (66, 67).

Intriguingly, as the conformation of apoA-I is different in each simulation performed in the present study, the notable differences in the fluctuations of apoA-I are possibly influenced by the conformation of the protein around the particle. As mentioned above, the conformation of apoA-I could depend on the size and lipid composition of the particles; in particular, the concentration of free cholesterol could be a critical determinant of apoA-I conformation as it was noticed by the simulations that cholesterol molecules favorably interact with apoA-I. Presumably, the conformation and dynamical properties of apoA-I around the HDL particles are constantly changing as the lipid and protein moieties vary. Therefore, producing any static or unified conformational data for apoA-I around the native HDL particles is very challenging. However, by means of state-of-the-art coarse-grained simulations we can now statistically define the most probable conformations of apoA-I induced by the different molecular compositions of HDL particles. However, note that we should carry out more simulations to give more statistical power to the conformational changes seen in the present simulations. Our main aim in this study was to include an apoA-I model that covers same surface area as native apoA-I in the HDL particles and that is able to play a role in lipid partitioning. For this reason, the protein tertiary structural differences seen in our simulation must be treated with certain caution. Notably, the fatty acyl chain saturation/desaturation degree of phospholipids may affect the lateral movement of apoA-I on the particle surface.


Levels of polyunsaturated fatty acid containing ether phospholipids, including ethanolamine plasmalogens, were elevated in the HDL fractions of subjects with low HDL-C. Not much is known about the PC ether lipids in HDL, and in contrast to PE ether lipids (68), unambiguous structural characterization of these lipids is at present not possible. PE plasmalogens are known to be more abundant in HDL compared with other lipoprotein fractions (7). Plasmalogens can serve as antioxidants against reactive oxygen species (ROS) and may prevent the oxidation of cholesterol (69). However, under oxidative stress, the arachidonic acid-containing plasmalogens, such as found in our study, become precursors of potent inflammatory mediators, such as leukotrienes and hydroxyicosatetraenoic acids (70). Together, the role of ether lipids in HDL function is likely complex and demands further investigation.

Sphingomyelin subspecies with different fatty acyl structures were higher in high HDL-C subjects. Interestingly, we also demonstrated that high HDL-C subjects have lower plasma TNF α as well as hs-CRP levels compared with those of low HDL-C subjects. This observation has important consequences when connected to sphingomyelin metabolism. A key event in atherogenesis is endothelial activation induced by a variety of stimuli, such as TNF- α , resulting in the expression of various adhesion proteins (71). The expression of adhesion proteins on activated endothelial

cells plays an essential role for the inflammatory processes in the pathogenesis of atherosclerosis (72). Elevated levels of TNF- α and hs-CRP indicate a low-grade inflammation that could cause several downstream effects, such as activation of sphingomyelinase activities, and affect endothelial cell function and development of atherosclerosis. Connection to sphingomyelin metabolism is important, and activation of acid sphingomyelinase has been extensively studied in the past decade. The enzyme is highly activated by TNF- α (73, 74) and might affect the lower SM content in HDL derived from low HDL subjects. This issue needs further studies, such as in vitro cell cultures with the isolated HDL particles derived from low and high HDL cholesterol subjects, to make further conclusions on the physiological performance of the particles.

The marked differences in HDL lipid profiles reported here were obtained from the extreme ends of HDL-C levels in a large population cohort. Because of the relatively small sample size, the comparison of low versus high HDL-C allowed us to minimize the effect of confounding factors and to study major differences. This approach helped us to extract the key compositional and structural features of HDL particles in the context of HDL-cholesterol that should be investigated further. To eliminate the confounding effect of variation in the amount of apoA-I protein, the HDL particles were modeled based on the conservative assumption that the number of apoA-I molecules per particle is the same in the high and low HDL-C groups. One should thus keep in mind that our simulation model may not correctly represent the virtual structure of HDL, in which different numbers of apoA-I are present. However, given that the observed increase of average apoA-I amount in high HDL-C subjects would only decrease the relative amount of triacylglycerols in high HDL-C subjects, the lipid spatial distribution differences between the high and low HDL-C subjects are likely even bigger than estimated by our simulations.

CONCLUSION

We detected many important lipid composition changes in subjects with high and low HDL-C. Elevated sphingomyelin in high HDL-C subjects confirms and provides additional evidence for the anti-inflammatory role of HDL. The lipid compositional changes also induced a surprising shift in the spatial distribution of triacylglycerols in subjects with low levels of HDL-C. The prevalence of TGs on the surface of HDL particles in these subjects may affect the heteroexchange of core lipids by CETP as well as facilitate their modification by hepatic lipase. Finally, our study suggests that combining molecular profiling of lipoproteins with dynamic modeling of lipoprotein structure is a powerful new strategy that may help elucidate the complexity of systemic lipid metabolism as well as facilitate efforts to invent novel therapeutic strategies. 

The authors are grateful to Pirkko Alha, Hannele Hilden, Ulla Lahtinen, Laura Lund, Jari Metso, Sari Nuutinen, Heli Nygren, Helinä Perttunen-Nio, and Harri Rissanen for their excellent laboratory work and help in data management.

REFERENCES

- Gordon, T., W. P. Castelli, M. C. Hjortland, W. B. Kannel, and T. R. Dawber. 1977. High density lipoprotein as a protective factor against coronary heart disease. The Framingham Study. *Am. J. Med.* **62**: 707–714.
- Chirovsky, D. R., V. Fedirko, Y. Cui, V. Sazonov, and P. Barter. 2009. Prospective studies on the relationship between high-density lipoprotein cholesterol and cardiovascular risk: a systematic review. *Eur. J. Cardiovasc. Prev. Rehabil.* **16**: 404–423.
- Cooney, M. T., A. Dudina, D. De Bacquer, L. Wilhelmsen, S. Sans, A. Menotti, G. De Backer, P. Jousilahti, U. Keil, T. Thomsen, et al. 2009. HDL cholesterol protects against cardiovascular disease in both genders, at all ages and at all levels of risk. *Atherosclerosis.* **206**: 611–616.
- van Leuven, S. I., E. S. Stroes, and J. J. Kastelein. 2008. High-density lipoprotein: a fall from grace? *Ann. Med.* **40**: 584–593.
- Watts, G. F., P. H. Barrett, and D. C. Chan. 2008. HDL metabolism in context: looking on the bright side. *Curr. Opin. Lipidol.* **19**: 395–404.
- Vaisar, T., S. Pennathur, P. S. Green, S. A. Gharib, A. N. Hoofnagle, M. C. Cheung, J. Byun, S. Vuletic, S. Kassim, P. Singh, et al. 2007. Shotgun proteomics implicates protease inhibition and complement activation in the antiinflammatory properties of HDL. *J. Clin. Invest.* **117**: 746–756.
- Wiesner, P., K. Leidl, A. Boettcher, G. Schmitz, and G. Liebisch. 2009. Lipid profiling of FPLC-separated lipoprotein fractions by electrospray ionization tandem mass spectrometry. *J. Lipid Res.* **50**: 574–585.
- Glass, C. K., and J. L. Witztum. 2001. Atherosclerosis: the road ahead. *Cell.* **104**: 503–516.
- Yancey, P. G., M. de la Llera-Moya, S. Swarnakar, P. Monzo, S. M. Klein, M. A. Connelly, W. J. Johnson, D. L. Williams, and G. H. Rothblat. 2000. High density lipoprotein phospholipid composition is a major determinant of the bi-directional flux and net movement of cellular free cholesterol mediated by scavenger receptor BI. *J. Biol. Chem.* **275**: 36596–36604.
- Brewer, H. B., Jr. 2004. Increasing HDL cholesterol levels. *N. Engl. J. Med.* **350**: 1491–1494.
- Nakanishi, S., R. Vikstedt, S. Soderlund, M. Lee-Rueckert, A. Hiukka, C. Ehnholm, M. Muilu, J. Metso, J. Naukkarinen, L. Palotie, et al. 2009. Serum, but not monocyte macrophage foam cells derived from low HDL-C subjects, displays reduced cholesterol efflux capacity. *J. Lipid Res.* **50**: 183–192.
- Wang, N., D. Lan, W. Chen, F. Matsuura, and A. R. Tall. 2004. ATP-binding cassette transporters G1 and G4 mediate cellular cholesterol efflux to high-density lipoproteins. *Proc. Natl. Acad. Sci. USA.* **101**: 9774–9779.
- Fournier, N., J-L. Paul, V. Atger, A. Cogny, T. Soni, M. de la Llera-Moya, G. Rothblat, and N. Moatti. 1997. HDL phospholipid content and composition as a major factor determining cholesterol efflux capacity from Fu5AH cells to human serum. *Arterioscler. Thromb. Vasc. Biol.* **17**: 2685–2691.
- Davidson, W. S., K. L. Gillotte, S. Lund-Katz, W. J. Johnson, G. H. Rothblat, and M. C. Phillips. 1995. The effect of high density lipoprotein phospholipid acyl chain composition on the efflux of cellular free cholesterol. *J. Biol. Chem.* **270**: 5882–5890.
- Vance, D. E., and J. E. Vance, editors. 2008. *Biochemistry of Lipids, Lipoproteins and Membranes.* Elsevier, Hungary.
- Kotronen, A., V. Velagapudi, L. Yetukuri, J. Westerbacka, R. Bergholm, K. Ekroos, J. Makkonen, M. R. Taskinen, M. Oresic, and H. Yki-Jarvinen. 2009. Serum saturated fatty acids containing triacylglycerols are better markers of insulin resistance than total serum triacylglycerol concentrations. *Diabetologia.* **52**: 684–690.
- Han, X., and R. W. Gross. 2005. Shotgun lipidomics: electrospray ionization mass spectrometric analysis and quantitation of cellular lipidomes directly from crude extracts of biological samples. *Mass Spectrom. Rev.* **24**: 367–412.
- Oresic, M., V. A. Hanninen, and A. Vidal-Puig. 2008. Lipidomics: a new window to biomedical frontiers. *Trends Biotechnol.* **26**: 647–652.
- Aromaa, A., and S. Koskinen, editors. 2004. Health and functional capacity in Finland: baseline results of the Health 2000 Health Examination Survey. National Public Health Institute, Helsinki, Finland.
- Taskinen, M. R., T. Kuusi, E. Helve, E. A. Nikkila, and H. Yki-Jarvinen. 1988. Insulin therapy induces antiatherogenic changes of serum lipoproteins in noninsulin-dependent diabetes. *Arteriosclerosis.* **8**: 168–177.

21. Blanche, P. J., E. L. Gong, T. M. Forte, and A. V. Nichols. 1981. Characterization of human high-density lipoproteins by gradient gel electrophoresis. *Biochim. Biophys. Acta.* **665**: 408–419.
22. Perusse, M., A. Pascot, J. P. Despres, C. Couillard, and B. Lamarche. 2001. A new method for HDL particle sizing by polyacrylamide gradient gel electrophoresis using whole plasma. *J. Lipid Res.* **42**: 1331–1334.
23. Vakkilainen, J., M. Jauhiainen, K. Ylitalo, I. O. Nuotio, J. S. Viikari, C. Ehnholm, and M. R. Taskinen. 2002. LDL particle size in familial combined hyperlipidemia: effects of serum lipids, lipoprotein-modifying enzymes, and lipid transfer proteins. *J. Lipid Res.* **43**: 598–603.
24. Friedewald, W. T., R. I. Levy, and D. S. Fredrickson. 1972. Estimation of the concentration of low-density lipoprotein cholesterol in plasma, without use of the preparative ultracentrifuge. *Clin. Chem.* **18**: 499–502.
25. Siggins, S., M. Jauhiainen, V. M. Olkkonen, J. Tenhunen, and C. Ehnholm. 2003. PLTP secreted by HepG2 cells resembles the high-activity PLTP form in human plasma. *J. Lipid Res.* **44**: 1698–1704.
26. Damen, J., J. Regts, and G. Scherphof. 1982. Transfer of [14C] phosphatidylcholine between liposomes and human plasma high density lipoprotein. Partial purification of a transfer-stimulating plasma factor using a rapid transfer assay. *Biochim. Biophys. Acta.* **712**: 444–452.
27. Jauhiainen, M., and C. Ehnholm. 2005. Determination of human plasma phospholipid transfer protein mass and activity. *Methods.* **36**: 97–101.
28. Siggins, S., M. Karkkainen, J. Tenhunen, J. Metso, E. Tahvanainen, V. M. Olkkonen, M. Jauhiainen, and C. Ehnholm. 2004. Quantitation of the active and low-active forms of human plasma phospholipid transfer protein by ELISA. *J. Lipid Res.* **45**: 387–395.
29. Groener, J. E., R. W. Pelton, and G. M. Kostner. 1986. Improved estimation of cholesteryl ester transfer/exchange activity in serum or plasma. *Clin. Chem.* **32**: 283–286.
30. Kleemola, P., R. Freese, M. Jauhiainen, R. Pahlman, G. Alfthan, and M. Mutanen. 2002. Dietary determinants of serum paraoxonase activity in healthy humans. *Atherosclerosis.* **160**: 425–432.
31. Geladi, P., and B. R. Kowalski. 1986. Partial least-squares regression: a tutorial. *Anal. Chim. Acta.* **185**: 1–17.
32. Barker, M., and W. Rayens. 2003. Partial least squares for discrimination. *J. Chemometr.* **17**: 166–173.
33. Wise, B. M., N. B. Gallagher, R. Bro, J. M. Shaver, W. Windig, and J. S. Koch. 2005. PLS Toolbox 3.5 for use with Matlab. Manson, WA, Eigenvector Research, Inc.
34. Wold, S., K. Esbensen, and P. Geladi. 1987. Principal component analysis. *Chemom. Intell. Lab. Syst.* **2**: 37–52.
35. Borhani, D. W., D. P. Rogers, J. A. Engler, and C. G. Brouillette. 1997. Crystal structure of truncated human apolipoprotein A-I suggests a lipid-bound conformation. *Proc. Natl. Acad. Sci. USA.* **94**: 12291–12296.
36. Segrest, J. P., M. K. Jones, A. E. Klon, C. J. Sheldahl, M. Hellinger, H. De Loof, and S. C. Harvey. 1999. A detailed molecular belt model for apolipoprotein A-I in discoidal high density lipoprotein. *J. Biol. Chem.* **274**: 31755–31758.
37. Okon, M., P. Frank, Y. Marcel, and R. Cushley. 2002. Heteronuclear NMR studies of human serum apolipoprotein A-I. Part I. Secondary structure in lipid-mimetic solution. *FEBS Lett.* **517**: 139–143.
38. Catte, A., J. C. Patterson, D. Bashtoyvy, M. K. Jones, F. Gu, L. Li, A. Rampioni, D. Sengupta, T. Vuorela, P. Niemelä, et al. 2008. Structure of spheroidal HDL particles revealed by combined atomistic and coarse-grained simulations. *Biophys. J.* **94**: 2306–2319.
39. Monticelli, L., S. K. Kandasamy, X. Periole, R. G. Larson, D. P. Tieleman, and S. J. Marrink. 2008. The MARTINI coarse-grained force field: extension to proteins. *J. Chem. Theory Comput.* **4**: 819–834.
40. Hess, B., C. Kutzner, D. van der Spoel, and E. Lindahl. 2008. GROMACS 4: algorithms for highly efficient, load-balanced, and scalable molecular simulation. *J. Chem. Theory Comput.* **4**: 435–447.
41. Marrink, S. J., H. J. Risselada, S. Yefimov, D. P. Tieleman, and A. H. de Vries. 2007. The MARTINI force field: coarse grained model for biomolecular simulations. *J. Phys. Chem. B.* **111**: 7812–7824.
42. Berendsen, H. J. C., J. P. M. Postma, W. F. van Gunsteren, A. DiNola, and J. R. Haak. 1984. Molecular dynamics with coupling to an external bath. *J. Chem. Phys.* **81**: 3684–3690.
43. Pietiläinen, K. H., M. Sysi-Aho, A. Rissanen, T. Seppänen-Laakso, H. Yki-Järvinen, J. Kaprio, and M. Orešić. 2007. Acquired obesity is associated with changes in the serum lipidomic profile independent of genetic effects—a monozygotic twin study. *PLoS ONE.* **2**: e218.
44. Lund-Katz, S., L. Liu, S. T. Thuanhai, and M. C. Phillips. 2003. High density lipoprotein structure. *Front. Biosci.* **8**: d1044–d1054.
45. Ibdah, J. A., and M. C. Phillips. 1988. Effects of lipid composition and packing on the adsorption of apolipoprotein A-I to lipid monolayers. *Biochemistry.* **27**: 7155–7162.
46. Sorci-Thomas, M. G., L. Curtiss, J. S. Parks, M. J. Thomas, M. W. Kearns, and M. Landrum. 1998. The hydrophobic face orientation of apolipoprotein A-I amphipathic helix domain 143-164 regulates lecithin:cholesterol acyltransferase activation. *J. Biol. Chem.* **273**: 11776–11782.
47. Cho, K-H., D. M. Durbin, and A. Jonas. 2001. Role of individual amino acids of apolipoprotein A-I in the activation of lecithin:cholesterol acyltransferase and in HDL rearrangements. *J. Lipid Res.* **42**: 379–389.
48. Rader, D. J. 2006. Molecular regulation of HDL metabolism and function: implications for novel therapies. *J. Clin. Invest.* **116**: 3090–3100.
49. Williamson, R., D. Lee, J. Hagaman, and N. Maeda. 1992. Marked reduction of high density lipoprotein cholesterol in mice genetically modified to lack apolipoprotein A-I. *Proc. Natl. Acad. Sci. USA.* **89**: 7134–7138.
50. Schaefer, E. J., W. H. Heaton, M. G. Wetzel, and H. B. Brewer, Jr. 1982. Plasma apolipoprotein A-I absence associated with a marked reduction of high density lipoproteins and premature coronary artery disease. *Arterioscler. Thromb. Vasc. Biol.* **2**: 16–26.
51. Weng, W., and J. L. Breslow. 1996. Dramatically decreased high density lipoprotein cholesterol, increased remnant clearance, and insulin hypersensitivity in apolipoprotein A-II knockout mice suggest a complex role for apolipoprotein A-II in atherosclerosis susceptibility. *Proc. Natl. Acad. Sci. USA.* **93**: 14788–14794.
52. Nakamura, Y., L. Kotite, Y. Gan, T. A. Spencer, C. J. Fielding, and P. E. Fielding. 2004. Molecular mechanism of reverse cholesterol transport: reaction of pre-beta-migrating high-density lipoprotein with plasma lecithin/cholesterol acyltransferase. *Biochemistry.* **43**: 14811–14820.
53. Watanabe, H., S. Soderlund, A. Soro-Paavonen, A. Hiukka, E. Leinonen, C. Alagona, R. Salonen, T-P. Tuomainen, C. Ehnholm, M. Jauhiainen, et al. 2006. Decreased high-density lipoprotein (HDL) particle size, prebeta-, and large HDL sub-species concentration in finnish low-HDL families: relationship with intima-media thickness. *Arterioscler. Thromb. Vasc. Biol.* **26**: 897–902.
54. Barter, P. J. 2002. Hugh Sinclair Lecture: The regulation and remodelling of HDL by plasma factors. *Atherosclerosis.* **3(Suppl.)**: 39–47.
55. Lamarche, B., K. D. Uffelman, A. Carpentier, J. S. Cohn, G. Steiner, P. H. Barrett, and G. F. Lewis. 1999. Triglyceride enrichment of HDL enhances in vivo metabolic clearance of HDL apo A-I in healthy men. *J. Clin. Invest.* **103**: 1191–1199.
56. Hammad, S. M., S. Stefansson, W. O. Twal, C. J. Drake, P. Fleming, A. Remaley, H. B. Brewer, and W. S. Argraves. 1999. Cubilin, the endocytic receptor for intrinsic factor-vitamin B12 complex, mediates high-density lipoprotein holoparticle endocytosis. *Proc. Natl. Acad. Sci. USA.* **96**: 10158–10163.
57. Kozyraki, R., J. Fyfe, M. Kristiansen, C. Gerdes, C. Jacobsen, S. Cui, E. I. Christensen, M. Aminoff, A. de la Chapelle, R. Krahe, et al. 1999. The intrinsic factor-vitamin B12 receptor, cubilin, is a high-affinity apolipoprotein A-I receptor facilitating endocytosis of high-density lipoprotein. *Nat. Med.* **5**: 656–661.
58. Kumpula, L. S., J. M. Kumpula, M-R. Taskinen, M. Jauhiainen, K. Kaski, and M. Ala-Korpela. 2008. Reconsideration of hydrophobic lipid distributions in lipoprotein particles. *Chem. Phys. Lipids.* **155**: 57–62.
59. Huuskonen, J., V. M. Olkkonen, M. Jauhiainen, and C. Ehnholm. 2001. The impact of phospholipid transfer protein (PLTP) on HDL metabolism. *Atherosclerosis.* **155**: 269–281.
60. Jiang, X., O. L. Francone, C. Bruce, R. Milne, J. Mar, A. Walsh, J. L. Breslow, and A. R. Tall. 1996. Increased prebeta-high density lipoprotein, apolipoprotein AI, and phospholipid in mice expressing the human phospholipid transfer protein and human apolipoprotein AI transgenes. *J. Clin. Invest.* **98**: 2373–2380.
61. Jiang, X. C., C. Bruce, J. Mar, M. Lin, Y. Ji, O. L. Francone, and A. R. Tall. 1999. Targeted mutation of plasma phospholipid transfer protein gene markedly reduces high-density lipoprotein levels. *J. Clin. Invest.* **103**: 907–914.

62. Föger, B., S. Santamarina-Fojo, R. Shamburek, C. Parrot, G. Talley, and H. Brewer. 1997. Plasma phospholipid transfer protein. adenovirus-mediated overexpression in mice leads to decreased plasma high density lipoprotein (HDL) and enhanced hepatic uptake of phospholipids and cholesteryl esters from HDL. *J. Biol. Chem.* **272**: 27393–27400.
63. Rye, K-A., M. Jauhiainen, P. J. Barter, and C. Ehnholm. 1998. Triglyceride-enrichment of high density lipoproteins enhances their remodelling by phospholipid transfer protein. *J. Lipid Res.* **39**: 613–622.
64. Cavigiolio, G., B. Shao, E. G. Geier, G. Ren, J. W. Heinecke, and M. N. Oda. 2008. The interplay between size, morphology, stability, and functionality of high-density lipoprotein subclasses. *Biochemistry.* **47**: 4770–4779.
65. Curtiss, L. K., D. J. Bonnet, and K-A. Rye. 2000. The conformation of apolipoprotein A-I in high-density lipoproteins is influenced by core lipid composition and particle size: a surface plasmon resonance study. *Biochemistry.* **39**: 5712–5721.
66. Bolin, D. J., and A. Jonas. 1996. Sphingomyelin inhibits the lecithin-cholesterol acyltransferase reaction with reconstituted high density lipoproteins by decreasing enzyme binding. *J. Biol. Chem.* **271**: 19152–19158.
67. Subbaiah, P. V., P. Horvath, and S. B. Achar. 2006. Regulation of the activity and fatty acid specificity of lecithin-cholesterol acyltransferase by sphingomyelin and its metabolites, ceramide and ceramide phosphate. *Biochemistry.* **45**: 5029–5038.
68. Zemski Berry, K. A., and R. C. Murphy. 2004. Electrospray ionization tandem mass spectrometry of glycerophosphoethanolamine plasmalogen phospholipids. *J. Am. Soc. Mass Spectrom.* **15**: 1499–1508.
69. Maeba, R., and N. Ueta. 2003. Ethanolamine plasmalogens prevent the oxidation of cholesterol by reducing the oxidizability of cholesterol in phospholipid bilayers. *J. Lipid Res.* **44**: 164–171.
70. Murphy, R. C. 2001. Free-radical-induced oxidation of arachidonoyl plasmalogen phospholipids: antioxidant mechanism and precursor pathway for bioactive eicosanoids. *Chem. Res. Toxicol.* **14**: 463–472.
71. Xia, P., J. R. Gamble, K-A. Rye, L. Wang, C. S. T. Hii, P. Cockerill, Y. Khew-Goodall, A. G. Bert, P. J. Barter, and M. A. Vadas. 1998. Tumor necrosis factor-alpha induces adhesion molecule expression through the sphingosine kinase pathway. *Proc. Natl. Acad. Sci. USA.* **95**: 14196–14201.
72. Ross, R. 1999. Atherosclerosis—an inflammatory disease. *N. Engl. J. Med.* **340**: 115–126.
73. García-Ruiz, C., A. Colell, M. Mari, A. Morales, M. Calvo, C. Enrich, and J. C. Fernández-Checa. 2003. Defective TNF-alpha-mediated hepatocellular apoptosis and liver damage in acidic sphingomyelinase knockout mice. *J. Clin. Invest.* **111**: 197–208.
74. Schütze, S., K. Potthoff, T. Machleidt, D. Berkovic, K. Wiegmann, and M. Krönke. 1992. TNF activates NF-kappaB by phosphatidylcholine-specific phospholipase C-induced “acidic” sphingomyelin breakdown. *Cell.* **71**: 765–776.